IHS Markit

Fault Enhancement and Visualization with 3D Log-Gabor Filter Array

Yingwei Yu, IHS Global, Inc.

SUMMARY

Many seismic attributes today reveal fault and fracture patterns. However, these fault attributes often suffer from noise or artifacts in the input data, resulting in data that is not high-enough a quality for automatic fault pickers to use directly without a post-attribute enhancement. In this paper, we introduce a new method to enhance the fault patterns in a 3D seismic volume using an array of 3D log-Gabor filters, which optimize fault planes by identifying isolated sections as a coherent fault or fracture while suppressing footprints, noise, and other artifacts. The resulting fault energy volume, which represents the enhanced faults, assists with fault interpretation. Unlike conventional fault enhancement, our method is inspired by the neuronal mechanism of orientation perception in the brain, and does not require fault orientations as input for filtering. Instead, fault dip and azimuth are two additional output attributes which are estimated during the filtering process, and are used for further orientation analysis or volumetric fault visualization. The proposed method is applied to real-world 3D seismic data located at *Great South Basin*, New Zealand offshore, which contains complex fault networks.

INTRODUCTION

In seismic interpretation, faults are important geologic structures. By definition, faults are planes or zones that are due to the earth's crust movements (Twiss and Moores, 2007). Unlike horizons, faults are not directly associated with geophysical events in the seismic data, such as peaks, troughs, or zero-crossing. Therefore, the higher-confidence interpretation of faults usually depends on seismic attributes, such as a similarity attribute (Michelena et al., 1998). These seismic attributes can be categorized into either *discontinuity*-based or *geometric*-based types.

The *discontinuity*-based attributes are sensitive either to abrupt changes, such as edges, or the degree of coherence of the seismic amplitudes. Aqrawi and Boe (2011) presented a dip-guided Sobel filter to highlight faults as edges in a 3D seismic volume. Chopra and Marfurt (2007) summarized different types of coherence attributes, including correlation (Bahorich and Farmer, 1995; Michelena et al., 1998), semblance (Marfurt et al., 1998, 1999), variance (Chopra and Marfurt, 2007), eigenstructure (Gersztenkorn and Marfurt, 1999), gradient structure tensor (GST)-based (Randen et al., 2000), and least-square-based (Bednar, 1998) types.

In addition, curvature and dip are *geometric*-based attributes that can indicate fault and fracture features. Lisle (1994) observed that there is a strong correlation between Gaussian curvatures and fractures. Chopra and Marfurt (2007) compared different curvature attributes, and concluded that the most-positive and most-negative curvatures correlate most closely to faults and fractures. Besides curvatures, many dip-based attributes are also good indicators of faults. Examples are instantaneous dip, dip variance, and smoothed dip of maximum similarity (Taner, 2001).

Fault Enhancement by Post-attribute Filters

Even though many seismic attributes as introduced above may be used to reveal fault patterns in a formation, the actual fault patterns may not be continuous, and a single fault may appear as a combination of seemingly isolated parts with noise or horizontal footprints. This makes it difficult for faults to be picked out automatically (Dorn and James, 2005; Dorn, 2007). Therefore we need a post-process step for the fault attributes generated, which serves three goals: (1) connecting isolated parts of a single fault together into an entire piece; (2) removing footprints in low-dips; and (3) improving S/N ratio of the seismic attribute. This post-processing step for fault attributes is *fault enhancement* (Dorn and James, 2005). The fault enhancement approaches can be grouped into two basic types of fixed orientation filtering or dynamic orientation scanning, based on their orientation-selecting parameter.

Fixed orientation filtering

The fixed orientation filtering method is based on the observations that faults are vertical or with high-dip, and the enhancement is along a given high-dip angle in 2D seismic slice. Gersztenkorn and Marfurt (1999) enhanced faults in 2D along a strictly vertical orientation, and Admasu et al. (2006) employed a 2D log-Gabor filter to highlight faults along a predefined dip as a parameter. The problems with this approach are: (1) faults in a volume are not strictly vertical but have various dips. A single dip only enhances faults of given angle; (2) the correct dip has to be estimated before filtering, and this could be time consuming and inconvenient to do for every fault; and (3) the filter only operates in 2D, so the faults' azimuth are often ignored.

Dynamic orientation scanning

In the scanning approach, fault angles are not pre-defined before smoothing, but estimated on-the-fly. Pedersen et al. (2002), and Zhe and Gu (2012) estimated the orientation field of 2D seismic coherence with a gradient-based method, and used an ant-colony algorithm to highlight the fault patterns along the dip orientations without pre-defined dip angles. Hale (2012, 2013) computed a fault likelihood volume through scanning the ridges in the volume over possible fault orientations, and Wu and Hale (2015) further extracted fault surfaces with this fault likelihood volume. Boe (2012) used a windowed 3D Radon filter to enhance fault surface patterns in an edge volume, and Wang and Alregib (2014) employed 3D Hough transform for the fault plane detection. The resulting enhanced fault surface is the plane with the maximal mean planar energy in all candidate orientations. The benefit of this approach is that multiple faults in one seismic attribute volume can be enhanced in a single pass without specifying the dip for each

fault. The azimuth and dip are outputs of the process, instead of the inputs.

Our proposed method belongs to the dynamic orientation filtering approach by using an array of 3D log-Gabor filters to scan fault planes in all possible orientations in 3D (Yu et al., 2015). The operation is performed in the frequency-wavenumber domain through 3D Fourier transform without any spatial window defined.

Motivation

The idea of using log-Gabor filter array was originally inspired from the neuronal circuits in the biological brain by simulating the robust mechanism in which humans perceive orientation patterns from a natural image.

As illustrated in figure 1, Hubel and Wiesel (1959) proposed an ice-cube model of the primary visual cortex. In the model, the visual cortex area is composed of a slab of orientation detectors (simple cells), which are tuned in the responses to different orientation patterns. The perceived angle in the visual input pattern is then determined by the strength of the orientation detectors' responses. Yu et al. (2011, 2013) applied the computational model of primary visual cortex with 2D log-Gabor filters to calculate the volumetric dip and azimuth of seismic data.

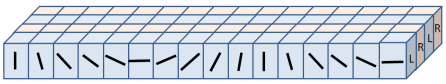

Figure 1: **The Orientation Columns in the Primary Visual Cortex.** Redrawn from Hubel and Wiesel (1959).

For the application of fault enhancements, we extended the orientation detectors from 2D to 3D, and employed an array of such filters to detect and enhance salient fault patterns in a seismic volume.

The next section introduces our methods to enhance the faults and derive the 3D orientation vector field using 3D log-Gabor filter array. Experiments and results follow in the third section.

METHODS

To enhance the fault planar structures in any fault attribute volume, we used an array of 3D log-Gabor filters. In the filter set, each filter is tuned to a certain dip and azimuth orientation. The input seismic attribute is then convolved with each filter in the array. This convolution associates each seismic sample point with a maximum filter response which in turn enhances linear planar structural patterns and forms a new seismic attribute - orientation energy. This attribute indicates fault distribution in the 3D seismic volume. The maximum response filter defines the fault dip and azimuth for each sample.

3D Log-Gabor Filter

The 3D log-Gabor filter is originally applied in image analysis as a feature detector (Dosil et al., 2006) , and in video processing for motion detection (Chamorro-Martinez et al., 2003), which is an extension to the 2-D log-Gabor filter. Field (1987) defined the 2-D log-Gabor filter in 2-D Fourier domain with radial and angular components:

$$H^{<\theta>}(f,q) = H_f(f) \times H_a^{<\theta>}(q), \tag{1}$$

where H_f is the frequency component, and $H_a^{<\theta>}$ the angular component. The frequency component is a Gaussian distribution in logarithmic scale:

$$H_f(f) = \exp\left(-\frac{ln^2(f/f_0)}{2ln^2(\sigma_f/f_0)}\right), \tag{2}$$

where f is frequency variable, σ_f the frequency standard deviation, and f_0 the central frequency constant.

Dosil et al. (2006) extended the 2-D log-Gabor into 3D by modifying the angular component with two angles of $<\theta,\phi>$, which are the azimuth and the dip parameters:

$$H_a^{<\theta,\phi>}(q) = \exp\left(-\frac{\|p(\theta,\phi),q\|}{2\sigma_\alpha^2}\right), \tag{3}$$

where q is a 3-D unit vector in frequency-wavenumber domain, and p is a unit vector, whose azimuth and dip are θ and ϕ. $\|.\|$ is an operator that returns the angle between two unit vectors. σ_α is the angular standard deviation, and we set it to $\frac{\pi}{24}$ in our experiments. Figure 2 illustrates the filter's central unit vector p in an angular component, $H_a^{<\theta,\phi>}$.

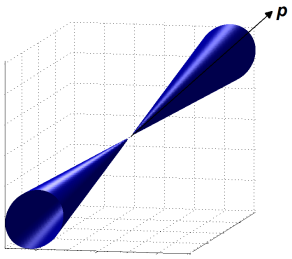

Figure 2: **Angular Component of 3D Log-Gabor Filter.** The angular component, illustrated with an iso-value of 0.5, is shown in a frequency-wavenumber domain. The central orientation vector p has azimuth $\theta = \frac{\pi}{4}$ and dip $\phi = \frac{\pi}{3}$. The angular standard deviation $\sigma_\alpha = \frac{\pi}{24}$.

When convolving with an input 3D volume, the 3D log-Gabor filter enhances the planar structure that is perpendicular to its central orientation vector p, and suppresses other planar patterns at different angles at various levels. The linear plane patterns that are parallel to the central vector p will be mostly suppressed.

Array of 3D Log-Gabor Filters

With a single 3D log-Gabor filter defined, we can construct an array of 3D log-Gabor filters that is indexed by the filters' dip ϕ and azimuth θ. In our implementation, θ and ϕ are assigned with a series of discrete values as follows.

$$\left\{H^{<\theta,\phi>} | \theta = [0^\circ, 10^\circ, ...350^\circ], \phi = [0^\circ, 2^\circ, ...30^\circ]\right\} \tag{4}$$

The procedure to enhance the fault attribute volume with the filter bank is as follows. We first convert the input volume $V(x,y,z)$ into a frequency-wavenumber domain by 3D Fourier transform $\hat{V}(u,v,w)$. For each 3D log-Gabor filter in the filter bank, we convolve it (the $*$ operator) with the input volume:

$$\hat{Y}^{<\theta,\phi>}(u,v,w) = H^{<\theta,\phi>} * \hat{V}(u,v,w), \tag{5}$$

Then by inverse Fourier transform, we convert $\hat{Y}^{<\theta,\phi>}(u,v,w)$ back into spatial domain as $Y^{<\theta,\phi>}(x,y,z)$. After convolution with every filter $H^{<\theta,\phi>}$ in the filter bank, we line up all the filter responses $Y^{<\theta,\phi>}(x,y,z)$. For an individual voxel at sample (x,y,z), we can derive the fault plane's orientation at this location, which is perpendicular to the central vector of maximum response filter (see Figure 3 for an illustration). The filter's azimuth α and dip β at voxel (x,y,z) are:

$$<\alpha,\beta> = \arg\max_{\theta,\phi} \left| Y^{<\theta,\phi>}(x,y,z) \right|, \tag{6}$$

where $|.|$ is the norm operator of the complex value. As illustrated in figure 3, the pair $<\alpha,\beta>$ represents the central vector p's azimuth and dip of the filter, which has the maximum response at location (x,y,z). The corresponding maximum response energy E for sample (x,y,z) is:

$$E(x,y,z) = \left| Y^{<\alpha(x,y,z),\beta(x,y,z)>}(x,y,z) \right|. \tag{7}$$

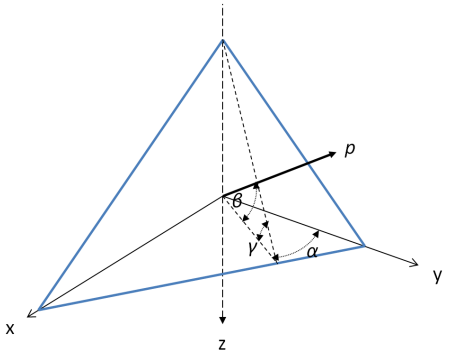

Figure 3: **Deriving Fault Dip and Azimuth from Filter.** The central angle vector p of the filter with the maximum response is perpendicular to the fault plane (blue) as shown. The vector p's azimuth α is the same as the fault's azimuth along its dip, while the fault's dip angle γ is complementary to the filter's dip β.

For fault enhancement, the orientation energy E represents the probability of faults. As demonstrated by figure 3, the fault plane's azimuth along its dip direction is the same as the filter central vector p's azimuth α, while the fault's dip γ (equation 8) is the complimentary angle of p's dip β.

$$\gamma(x,y,z) = \frac{\pi}{2} - \beta(x,y,z) \tag{8}$$

In summary, we can enhance a fault attribute by convolving with 3D log-Gabor filter array $\left\{H^{<\theta,\phi>}\right\}$, with the result containing three attributes: the energy E (equation 7), azimuth γ (equation 8), and dip α (equation 6).

EXPERIMENTS AND RESULTS

The described algorithm was tested on a 3D seismic survey of the *Great South Basin* located southeast offshore New Zealand. Figure 4 shows a vertical slice from this survey, with an array of faults. The workflow to enhance and analyze the fault patterns in the volume contains three steps.

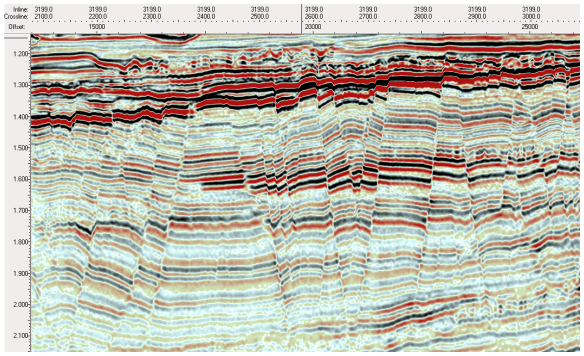

Figure 4: **Seismic survey from the *Great South Basin* located southeast New Zealand offshore.** An array of faults is evident. The shallow region has strong amplitudes and higher contrast, while in the lower region, the amplitudes are relatively weaker.

Step 1: Generate the symmetry attribute.

The first step is to generate a *Symmetry* attribute (patent pending) to reveal faults from the seismic amplitude data. To calculate this attribute, for each sample in the volume, we evaluate the 180-degree rotational symmetry in its neighborhood. The neighborhood is defined by a 3D cylindrical window, which is corrected by the apparent dip angles in both inline and crossline directions using a 2D log-Gabor filter array.

Figure 5 shows the symmetry attribute in which faults are visible. Note that in this survey, the shallow region above 1.5s has strong amplitudes and high contrast, while in the lower region (below 1.8s), the amplitudes are relatively weak. Symmetry works well under both conditions due to the normalization term in the equation.

Step 2: Fault Enhancement with 3D log-Gabor filter array.

To enhance the linear fault patterns, and improve the S/N ratio, we convolved the symmetry volume with a 3D log-Gabor filter array as described in the previous section. The 3D log-Gabor filter array parameters are configured the same as in figure 2 and equation 4. The convolution yields three volumetric attributes: fault energy, fault dip, and fault azimuth. Figure 6 shows enhanced fault energy using symmetry in figure 5 as an input. Note that the isolated fault segments are more connected, and noise is significantly suppressed in the enhanced volume.

For using fault attributes other than symmetry attribute as input, see a case study of the same New Zealand dataset, which compared the fault enhancement with various seismic attributes as input (Yu and Mardanova, 2016).

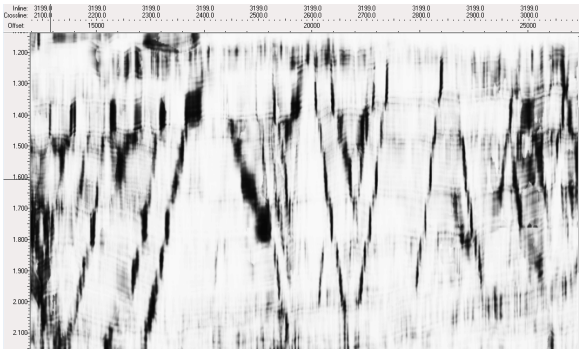

Figure 5: **Symmetry attribute.** Results of symmetry using seismic survey as shown in figure 4. Faults are more visible. The symmetry attribute is not only sensitive to the region with higher amplitudes, but also at the weaker part.

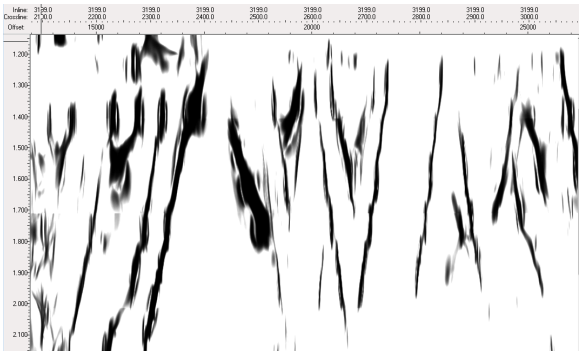

Figure 6: **Fault energy attribute.** The fault patterns are enhanced by the orientation energy output from the 3D log-Gabor filter array. The input is the Symmetry attribute as shown in figure 5. Note that the isolated fault segments are in a more connected pattern, and noise is significantly suppressed.

Step 3: Orientation statistics and fault visualization.

To visualize faults in a volume, we rendered these fault attributes using color-coblending and opacity control techniques. As shown in figure 7, fault energy (figure 6) is co-blended with azimuth attribute. To hide the non-fault voxels, all samples with fault energy less than a threshold, say 0.1, are rendered in transparent. The color of the faults are defined by their corresponding azimuth attribute values.

In addition, with fault dip and azimuth attributes generated, we can run statistics on the orientation distribution for a given region. At the upper-left in figure 7, the azimuth distribution of the yellow rectangle on the top horizontal surface (at 1.604s) is presented by a rose diagram.

CONCLUSION

In conclusion, using an array of 3D log-Gabor filters can effectively enhance complex planar patterns in a fault-related attribute volume. The resulting energy attribute presents smoother

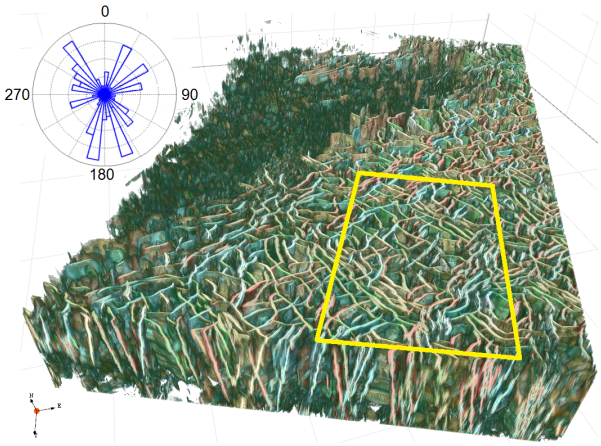

Figure 7: **Visualization of enhanced volumetric fault attributes generated by the 3-D log-Gabor array.** The volumetric attribute *orientation energy* is color-coblended with the *fault azimuth* attribute and proper opacity control (orientation energy cutoff value 0.1). The faults highlighted in this figure are color-coded by their azimuths. The rose diagram on the upper left shows the azimuth distribution within the yellow rectangle on the top horizontal slice at 1.604s.

and cleaner lines in both horizontal and vertical slices with sharper contrast when compared with the input attribute. In addition, fault dip and azimuth are estimated for the full volume at the same time, and these attributes can be used for orientation analysis, to enhance the fault volume visualization effects, and assist the fault interpretation process.

ACKNOWLEDGMENTS

Thanks to Irina Mardanova, Gary Jones, and Clifford Kelley for helpful discussions, and Sandra Rimmer for editing this paper. Thanks to New Zealand Petroleum & Minerals for the permission to use the seismic data in this work. The methods described in this paper are protected by US patent 9,105,075 (Yu et al., 2015). The authors would like to thank IHS for the support and permission to publish this paper.

REFERENCES

Admasu, F., S. Back, and K. Toennies, 2006, Autotracking of faults on 3d seismic data: Geophysics, **71(6)**, A49–A53.

Aqrawi, A. A., and T. H. Boe, 2011, Improved fault segmentation using a dip guided and modified 3d sobel filter: 81st Annual International Meeting of Society of Exploration Geophysicists, SEG Expanded Abstracts, Society of Exploration Geophysicists, 999–1003.

Bahorich, M. S., and S. L. Farmer, 1995, 3-d seismic coherency for faults and stratigraphic features: The Leading Edge, **14**, 1053–1058.

Bednar, J. B., 1998, Least-squares dip and coherence attributes: The Leading Edge, **17**, 775–776.

Boe, T., 2012, Enhancement of large faults with a windowed 3d radon transform filter: Annual International Meeting. SEG Expanded Abstract.

Chamorro-Martinez, J., J. Fdez-Valdivia, J. Garcia, and J. Martinez-Baena, 2003, A frequency-domain approach for the extraction of motion patterns: IEEE International Conference on Acoustics, Speech and Signal Processing (ICASSP-2003), Hong Kong, 165–168.

Chopra, S., and K. J. Marfurt, 2007, Seismic attributes for prospect identification and reservoir characterization: Societry of Exploration Geophysicists.

Dorn, G., 2007, Automated fault extraction (afe): American Association Petroleum Geologists Annual Convention and Exhibition (AAPG 2007), Long Beach, CA, AAPG, 5.

Dorn, G., and H. James, 2005, Automatic fault extraction of faults and a salt body in a 3-d survey from the eugene island area, gulf of mexico: Presented at the AAPG International Conference and Exhibition, Expanded Abstracts 19, AAPG.

Dosil, R., X. M. Pardo, and X. R.Fdez-Vidal, 2006, Data-driven synthesis of composite-feature detectors for 3d image analysis: Image and Vision Computing, **24**, 225 – 238. (3D Log-Gabor filter).

Field, D. J., 1987, Relations between the statistics of natural images and the response properties of cortical cells: J. Opt. Soc. Am. A, 2379–2394.

Gersztenkorn, A., and K. J. Marfurt, 1999, Eigenstructure based coherence computations as an aid to 3-d structual and stratigraphic mapping: Geophysics, **64**, 1468–1479.

Hale, D., 2012, Fault surfaces and fault throws from 3d seismic images: Annual International Meeting. SEG Expanded Abstract.

———, 2013, Methods to compute fault images, extract fault surfaces, and estimate fault throws from 3d seismic images: Geophysics, **78(2)**, O33–O43.

Hubel, D. H., and T. N. Wiesel, 1959, Receptive fields of single neurones in the cat's striate cortex: Journal of Physiololgy, **150**, 91–104.

Lisle, R. J., 1994, Detection of zones of abnormal strains in structures using gaussian curvature analysis: AAPG Bulletin, **78**, 1811–1819.

Marfurt, K. J., R. L. Kirlin, S. H. Farmer, and M. S. Bahorich, 1998, 3-d seismic attributes using a running window semblance-based algorithm: Geophysics, **63**, 1150–1165.

Marfurt, K. J., V. Sudhakar, A. Gersztenkorn, K. D. Crawford, and S. Nissen, 1999, Coherency calculations in the presence of structual dip: Geophysics, **64**, 104–111.

Michelena, R., S. M. E. Gonzlez, and M. C. de P., 1998, Similarity analysis: A new tool to summarize seismic attributes information: The Leading Edge, **17(4)**, 545–548.

Pedersen, S., T. Randen, L. Sonneland, and O. Steen, 2002, Automatic fault extraction using artificial ants: 72nd Annual International Meeting. SEG Expanded Abstract, 512–515.

Randen, T., E. monsen, C. Signer, A. Abrahamsen, J. Hansen, T. Saeter, and J. Schlaf, 2000, Three-dimensional textural attributes for seismic data analysis: 70th Annual International Meeting. SEG Expanded Abstract, **19**, 668–671.

Taner, T., 2001, Seismic attributes: CSEG Recorder, **26(7)**, 48–56.

Twiss, R. J., and E. M. Moores, 2007, Structural geology, 2nd ed.: W. H. Freeman and Company.

Wang, Z., and G. Alregib, 2014, Automatic fault surface detection by using 3d hough transform: Annual International Meeting. SEG Expanded Abstract, 1439–1444.

Wu, X., and D. Hale, 2015, 3d seismic image processing for faults: Annual International Meeting. SEG Expanded Abstract.

Yu, Y., C. Kelley, and I. Mardanova, 2011, Automatic horizon picking in 3d seismic data using optical filters and minimum spanning tree: 81st Annual International Meeting of Society of Exploration Geophysicists, SEG Expanded Abstracts, Society of Exploration Geophysicists, 965–958.

———, 2013, Volumetric seismic dip and azimuth estimation with 2d log-gabor filter array: Annual International Meeting. SEG Expanded Abstract, 1357–1362.

———, 2015, Enhancing seismic features using an optical filter array: US Patent 9105075.

Yu, Y., and I. Mardanova, 2016, I3d attribute enhances fault recognition in seismic data: Presented at the EAGE International Conference & Exhibition 2016, Saint Petersburg, Russia (to appear).

Zhe, Y., and H. Gu, 2012, An automatic fault tracking approach based on ant colony algorithm: Annual International Meeting. SEG Expanded Abstract.